View metadata, citation and similar papers at core.ac.uk

brought to you by CORE

provided by Digital.CSIC

Component dynamics in polyvinylpyrrolidone concentrated aqueous solutions

Rémi Busselez, Arantxa Arbe, Silvina Cerveny, Sara Capponi, Juan Colmenero, and Bernhard Frick

Citation: The Journal of Chemical Physics **137**, 084902 (2012); doi: 10.1063/1.4746020

View online: http://dx.doi.org/10.1063/1.4746020

View Table of Contents: http://scitation.aip.org/content/aip/journal/jcp/137/8?ver=pdfcov

Published by the AIP Publishing

Articles you may be interested in

On the hydration of the phosphocholine headgroup in aqueous solution
J. Chem. Phys. **133**, 145103 (2010); 10.1063/1.3488998

Intermolecular momentum transfer in poly(perfluorosulfonic acid) membrane hydrated by aqueous solution of methanol: A molecular dynamics simulation study
J. Chem. Phys. **131**, 224901 (2009); 10.1063/1.3271829

Investigations on the structure of dimethyl sulfoxide and acetone in aqueous solution
J. Chem. Phys. **127**, 174515 (2007); 10.1063/1.2784555

Molecular dynamics and interactions of aqueous and dichloromethane solutions of polyvinylpyrrolidone
J. Chem. Phys. **125**, 034904 (2006); 10.1063/1.2208356

Ions in water: The microscopic structure of a concentrated HCl solution
J. Chem. Phys. **121**, 7840 (2004); 10.1063/1.1801031

This article is copyrighted as indicated in the article. Reuse of AIP content is subject to the terms at: http://scitation.aip.org/termsconditions. Downloaded to IP: 161.111.180.191 On: Fri, 05 Sep 2014 09:36:11

Component dynamics in polyvinylpyrrolidone concentrated aqueous solutions

Rémi Busselez,[1] Arantxa Arbe,[2,a)] Silvina Cerveny,[2] Sara Capponi,[3] Juan Colmenero,[4] and Bernhard Frick[5]

[1]*Donostia International Physics Center, Paseo Manuel de Lardizabal 4, E-20018 San Sebastián, Spain*
[2]*Centro de Física de Materiales (CSIC, UPV/EHU) and Materials Physics Center MPC, Paseo Manuel de Lardizabal 5, E-20018 San Sebastián, Spain*
[3]*Donostia International Physics Center, Paseo Manuel de Lardizabal 4, E-20018 San Sebastián, Spain and Departamento de Física de Materiales (UPV/EHU), Apartado 1072, E-20080 San Sebastián, Spain*
[4]*Centro de Física de Materiales (CSIC, UPV/EHU) and Materials Physics Center (MPC), Paseo Manuel de Lardizabal 5, E-20018 San Sebastián, Spain and Donostia International Physics Center, Paseo Manuel de Lardizabal 4, E-20018 San Sebastián, Spain*
[5]*Institut Laue–Langevin, BP 156, 38042 Grenoble Cedex 9, France*

(Received 7 June 2012; accepted 1 August 2012; published online 22 August 2012)

^{2}H-nuclear magnetic resonance (NMR) and neutron scattering (NS) on isotopically labelled samples have been combined to investigate the structure and dynamics of polyvinylpyrrolidone (PVP) aqueous solutions (4 water molecules/monomeric unit). Neutron diffraction evidences the nanosegregation of polymer main-chains and water molecules leading to the presence of water clusters. NMR reveals the same characteristic times and spectral shape as those of the slower process observed by broadband dielectric spectroscopy in this system [S. Cerveny *et al.*, J. Chem. Phys. **128**, 044901 (2008)]. The temperature dependence of such relaxation time crosses over from a cooperative-like behavior at high temperatures to an Arrhenius behavior at lower temperatures. Below the crossover, NMR features the spectral shape as due to a symmetric distribution of relaxation times and the underlying motions as isotropic. NS results on the structural relaxation of both components–isolated via H/D labeling–show (i) anomalously stretched and non-Gaussian functional forms of the intermediate scattering functions and (ii) a strong dynamic asymmetry between the components that increases with decreasing temperature. Strong heterogeneities associated to the nanosegregated structure and the dynamic asymmetry are invoked to explain the observed anomalies. On the other hand, at short times the atomic displacements are strongly coupled for PVP and water, presumably due to H-bond formation and densification of the sample upon hydration. © *2012 American Institute of Physics*. [http://dx.doi.org/10.1063/1.4746020]

I. INTRODUCTION

Polyvinylpyrrolidone (PVP) is one of the most widely used synthetic polymers in pharmaceutical, cosmetic, and food industries.[1–3] It can be found, e.g., in coatings, adhesives, as a binder in many pharmaceutical tablets or as a food additive (thickener E1201). Two properties of PVP are key ingredients for such technological interest: non-toxicity[4] and high solubility in several organic solvents (such as ethanol, acetic acid, or some alcohols among others) and water. The latter property is due to the possibility of H-bond formation between its carbonyl group and the hydroxyl groups of the solvents.

Motivated by the wide range of applications, PVP and complexes based on it have been subject of a large number of studies during the last years (see, e.g., Refs. 5–26). In a previous work,[27] some of us have investigated PVP/water mixtures driven also by a basic-science point of view, namely, trying to contribute to the understanding of the dynamics of supercooled water. The reason is that water crystallization can be inhibited in polymer solutions at sufficiently high polymer concentration, likely because the H-bonding network of water molecules is somehow restricted by the polymer matrix. This allows the study of water dynamics in the so-called "no-man's" land, where bulk water unavoidably crystallizes. Due to the big dipole moment of water molecule, broadband dielectric spectroscopy (BDS) is a very suitable technique to address its reorientational dynamical behavior in a wide frequency range. The BDS study previously carried out in PVP/water mixtures[27] revealed two dynamical processes of water. The faster (and weaker) one shows an Arrhenius-like behavior and was tentatively related with the dynamics of isolated water molecules likely directly bounded to the polymer. The temperature dependence of the characteristic times of the slower (and main) relaxation process exhibits a crossover from non-Arrhenius to Arrhenius behavior during cooling throughout the glass transition range. It is worth recalling that this peculiar feature of the dielectric response of water seems to be universal in solutions of hydrophilic polymers, biopolymers, and small glass-forming materials.[28] The vitrification of the slow component of the mixtures–of PVP in this case–was invoked as the reason of the emergence of confinement effects leading to the observed crossover in such systems.

a)Electronic mail: a.arbe@ehu.es.

 © 2012 American Institute of Physics

This article is copyrighted as indicated in the article. Reuse of AIP content is subject to the terms at: http://scitation.aip.org/termsconditions. Downloaded to IP: 161.111.180.191 On: Fri, 05 Sep 2014 09:36:11

In this work, we have extended our investigation of the PVP/water system by using neutron scattering (NS) and ^{2}H-nuclear magnetic resonance (NMR) techniques on isotopically labelled samples. Thereby we have addressed not only the water component dynamics–as with the previous BDS work–but also the motions of the polymer and the structural properties as well. The use of deuterium substitution has been crucial for our goal: (i) Neutron diffraction on isotopically labelled samples has accessed different partial structure factors, providing valuable insight in the structure of the mixture. The proposed existence of water clusters in the system (we have focused on a sample with 40 wt. % water concentration) based on BDS (Ref. 27) has been confirmed. (ii) Quasielastic neutron scattering (QENS) has allowed us selectively following the dynamics of both components. Since the incoherent cross section of hydrogen is much larger than any cross section of the other atoms conforming the system, in particular of deuterium, the scattered intensity is dominated by the incoherent contribution from the hydrogens in the sample. Thus, experiments on a sample with deuterated water provide selective information on the PVP component (in particular, about the self-motions of its protons). It is worth noting that the dynamics of the polymer component cannot be addressed by BDS. We also recall that the accessed scattering functions are related with the total atomic displacements, i.e., contain both translational and rotational modes. Since deuterated PVP was not available we could deduce the information on the water component from the analysis of the results on the fully protonated sample (which contains the contributions from protons in both, water and PVP) and considering the knowledge previously obtained for the PVP component. The backscattering instrument used for these measurements accesses the dynamics with $\approx$1 μeV resolution. (iii) From elastic fixed window neutron scans with 8 μeV resolution we have followed the temperature dependence of the proton displacements at $t \approx 0.5$ ns on the same samples. (iv) Finally, ^{2}H-NMR has accessed the reorientations of the O–D bond of heavy water in the mixture. This information is thus directly comparable to that obtained from BDS; in addition, hints about the isotropic character of the motions involved and the possibly underlying distribution of characteristic times can be deduced.

II. EXPERIMENTAL

A. Samples

PVP in aqueous solution (water concentration: 55 wt. %) was purchased from Aldrich Chemical and used without any further purification. The reported weight-average molecular weight (M_w) of this polymer is 160 000 g mol^{-1}. In order to prepare the solutions, the as received sample was first dehydrated by evaporating the water in a vacuum oven at 400 K during a week. Dried samples were then rehydrated by incorporating H_2O or D_2O in the appropriated concentration. The solutions were kept in sealed bottles during 5 days in order to achieve equilibrium. The systems investigated contained 40 wt. % water concentration and 42 wt. % water concentration for H_2O or D_2O, respectively. With the aforementioned concentrations, the number of water molecules per monomeric unit (n_w) is equal to 4 in both samples. We also investigated the structure of samples containing $n_w = 2$ deuterated water molecules/monomeric unit, corresponding to 22 wt. % D_2O water concentration.

The glass transition temperature of dry PVP and the mixture with 40 wt. % of water have been reported to be, respectively, $T_{g_{Dry}}^{onset} = 445$ K and $T_{g_{40wt.\%}}^{onset} = 218.5$ K.[27] We note however that in that paper the T_g was defined as the low-temperature onset of the ΔC_p marking the glass-transition process. These onset-T_gs correspond to conventional (defined as the middle point of ΔC_p) T_g-values of $T_{g_{Dry}} = 447$ K and $T_{g_{40wt.\%}} = 232$ K. Calorimetric measurements on the sample with deuterated water revealed $T_{g_{42wt.\%D_2O}} = 237$ K, i.e., 5° higher than in the fully protonated sample (see below, Fig. 7(a)). For neutron scattering studies, samples were prepared directly in aluminium flat holders. The thicknesses of the holders were chosen to assure more than 90% of transmission (i.e., 0.2 mm for the pure polymer and H_2O-hydrated samples and 0.4 mm for the PVP hydrated with D_2O). Samples for NMR studies were prepared directly in glass tubes of 5 mm of diameter. The tubes were sealed and kept at room temperature during 1 week to obtain homogeneous samples.

B. Neutron scattering

The magnitude measured in general in a NS experiment is the double differential scattering cross section, i.e., the neutron intensity scattered into a solid angle between Ω and $\Omega + d\Omega$, after having exchanged an energy between $\hbar\omega$ and $\hbar\omega + d\hbar\omega$ with the sample. This function provides information on the dynamics and structure of the sample. The measured cross section contains incoherent and coherent contributions. The coherent differential scattering cross section (i.e., integrated over all possible energy transfers) can be written as

$$\left(\frac{\partial\sigma}{\partial\Omega}\right)_{coh} = \frac{1}{N}\left\langle \sum_{i,j=1}^{N} \overline{b}_i\, \overline{b}_j e^{i\vec{Q}\vec{r}_{ij}} \right\rangle, \tag{1}$$

where b_i is the neutron coherent scattering length of atom i, N is the number of atoms, $\vec{r_{ij}} = \vec{r_i} - \vec{r_j}$ is the vector connecting the positions of atoms i and j at the same time and the brackets express the thermal average. The modulus of the momentum transfer Q is determined by the scattering angle θ and the wavelength of the incoming neutrons λ as $Q = 4\pi\, sin(\theta/2)/\lambda$. Thus, the differential coherent cross section reveals structural information (Fourier transform of the atomic pair distribution functions, weighed by the corresponding scattering lengths). In the limit $Q \to \infty$ this function is determined by the total coherent cross section σ_{coh}^{tot},

$$\left(\frac{\partial\sigma}{\partial\Omega}\right)_{coh} = \frac{1}{N}\sum_{i=1}^{N}\overline{b}_i^2 = \frac{1}{4\pi N}\sum_{i=1}^{N}\sigma_{coh}^{i} = \frac{\sigma_{coh}^{tot}}{4\pi}. \tag{2}$$

We note that x-ray diffraction also accesses the structural features through an equation similar to Eq. (1), but with Q-dependent scattering form factors instead. On the other hand, the incoherent differential scattering cross section does not depend on Q and is determined by the total incoherent cross

This article is copyrighted as indicated in the article. Reuse of AIP content is subject to the terms at: http://scitation.aip.org/termsconditions. Downloaded to IP: 161.111.180.191 On: Fri, 05 Sep 2014 09:36:11

TABLE I. Coherent scattering lengths and cross sections of the isotopes involved in the samples.

Isotope α	$\overline{b_\alpha}$ (fm)	σ^α_{coh}(barns)	σ^α_{inc}(barns)
H	− 3.7406	1.7583	80.27
D	6.671	5.592	2.05
^{12}C	6.6511	5.559	0
^{16}O	5.803	4.232	0
^{14}N	9.37	11.03	0.50

section σ^{tot}_{inc},

$$\left(\frac{\partial\sigma}{\partial\Omega}\right)_{inc} = \frac{1}{4\pi N}\sum_{i=1}^{N}\sigma^i_{inc} = \frac{\sigma^{tot}_{inc}}{4\pi}. \quad (3)$$

In Eqs. (2) and (3) we have introduced the cross sections of the atom i, σ^i_{inc}, and $\sigma^i_{coh} = (\overline{b_i})^2$. They depend on which kind of isotope α (α: H, D, C, O, ...) is the given nucleus i (see Table I). Incoherent scattering does not provide structural information but refers to single particle features. The $\hbar\omega$ and Q-dependencies of the incoherent contribution to the double differential cross section are determined by the incoherent scattering function. For a given isotope α, the incoherent scattering function $S^\alpha_{inc}(Q,\omega)$ is the Fourier transform of the intermediate incoherent scattering function $S^\alpha_{inc}(Q,t)$ and the double Fourier transform of $S^\alpha_{inc}(Q,\omega)$ yields the self-part of the Van Hove correlation function $G^\alpha_{self}(r,t)$,

$$G^\alpha_{self}(r,t) = \frac{1}{N_\alpha}\left\langle\sum_{i=1}^{N_\alpha}\delta[r - |\vec{r}_i(t) - \vec{r}_i(0)|]\right\rangle, \quad (4)$$

where N_α is the number of nuclei of the considered kind of isotope α in the sample. In the classical limit, $G^\alpha_{self}(r,t)$ is the probability of a given nucleus of kind α to be at distance r from the position where it was located at a time t before. Incoherent scattering looks at correlations between the positions of the same nucleus at different times.

The neutron scattering cross sections and scattering lengths for the different isotopes involved in the chemical formulae of PVP, H_2O, and D_2O are listed in Table I. Table II shows the cross sections for the samples investigated. In all the cases, the scattered intensity is dominated by the incoherent contribution from hydrogens and thereby provides information about the self-motion of such atoms, $S^H_{inc}(Q,\omega)$.

1. Diffraction with polarization analysis

Polarization analysis allows to separate experimentally the spin-coherent and spin-incoherent contributions to the neutron scattered intensity.[29,30] This technique provides valuable structural information even using samples with little coherent scattering,[31–33] as those here investigated. Contrarily to the coherent scattering, which does not induce a spin flip, incoherent scattering of a sample constituted of aleatory oriented spins has a 2/3 probability to spin flip the scattered neutrons. Hence, the separation of incoherent and coherent nuclear scattering processes can be achieved using a polarized incident neutron beam and counting separately the neutrons scattered with and without spin-flip with regard to the incident beam polarization, obtaining two different Q-dependent intensities: the spin flip intensity $I_{SF}(Q)$ and the non-spin flip intensity $I_{NSF}(Q)$.

Diffraction with polarization analysis measurements have been realized on the D7 instrument[34] at the Institute Laue-Langevin (ILL) in Grenoble in diffraction mode. We used $\lambda = 4.8$ Å. For this wavelength, the Q-range covered by the 132 detectors extends from 0.09 Å^{-1} to 2.5 Å^{-1}. We investigated both samples with $n_w = 4$ water molecules/monomer unit and the sample with $n_w = 2$ D_2O molecules/monomeric unit, at room temperature. Measuring times of 1 h for non-spin flip and 30 min for spin flip were employed. The raw data were corrected for detector efficiency, flipping ratio, sample container, empty cryostat, and absorption using ILL standard programs, leading to the corrected $I_{SF}(Q)$ and $I_{NSF}(Q)$ intensities. From these, the ratio between the coherent and incoherent scattering cross sections can easily be calculated:

$$\frac{\left(\frac{\partial\sigma}{\partial\Omega}\right)_{coh}(Q)}{\left(\frac{\partial\sigma}{\partial\Omega}\right)_{inc}(Q)} = \frac{I_{NSF}(Q) - \frac{1}{2}I_{SF}(Q)}{\frac{3}{2}I_{SF}(Q)}. \quad (5)$$

This procedure has the advantage to directly correct the coherent scattering function from Debye-Waller factor and instrumental effects.

2. Quasielastic neutron scattering

In a backscattering spectrometer, the instrumental resolution is optimized by using backscattering geometry.[35] In this work, we used the IN16 instrument[36] at the ILL to investigate the samples with $n_w = 4$ water molecules/monomeric unit. A standard configuration was chosen, with Si(111) monochromator and analyzers in backscattering geometry, which corresponds to $\lambda = 6.271$ Å. In this configuration IN16 offers an energy resolution (full width at half maximum) of 0.9 μeV with a nearly Gaussian shape and covers a Q-range from 0.2 to 1.9 Å^{-1}. The resolution function $R(Q,\omega)$ was determined from the measurement of a sample at 2 K, where the scattering is considered elastic in this experimental window.

TABLE II. Cross sections of the samples investigated. $\sigma^{Hs}_{inc}/\sigma_{tot}$ is the ratio between the incoherent cross section from all the hydrogens in the sample and the total (coherent + incoherent) cross section.

Sample	Unit	σ^{tot}_{coh}(barns/unit)	σ^{tot}_{inc}(barns/unit)	$\sigma^{tot}_{coh}/\sigma^{tot}_{inc}$	$\sigma^{Hs}_{inc}/\sigma_{tot}$
PVP	C_6H_9ON	64.367	722.94	0.089	0.9 176
PVP/D_2O ($n_w = 4$)	$C_6H_9ON + 4D_2O$	126.03	739.34	0.17 046	0.8 348
PVP/D_2O ($n_w = 2$)	$C_6H_9ON + 2D_2O$	95.199	731.14	0.13 021	0.87 426
PVP/H_2O ($n_w = 4$)	$C_6H_9ON + 4H_2O$	95.361	1365.1	0.069 857	0.93 436

This article is copyrighted as indicated in the article. Reuse of AIP content is subject to the terms at: http://scitation.aip.org/termsconditions. Downloaded to IP: 161.111.180.191 On: Fri, 05 Sep 2014 09:36:11

The acquired data were corrected for detector efficiency, sample container, and absorption using the standard programs available at ILL, thus finally providing the experimental scattering function $S_{exp}(Q, \omega)$. As above mentioned, for our samples it can be assumed that $S_{exp}(Q, \omega) \approx S^{H}_{exp}(Q, \omega)$, i.e., it corresponds to the incoherent scattering function of the hydrogens in the sample.

3. Elastic fixed windows scans

In elastic fixed window scans (EFWS) the energies of the incident and the detected neutrons after interacting with the sample are identical, and the recorded intensity only includes the purely elastic term $S_{inc}(Q, \omega = 0)$. However, dependent on the finite instrumental resolution, $R(Q, \omega)$, the EFWS intensities also contain quasielastic contributions with energy transfers smaller than the resolution of the spectrometer $\delta\hbar\omega$ (amplitude of the quasielastic signal at $\delta\hbar\omega \approx 0$).

The EFWS were carried out by the IN13 backscattering spectrometer at the ILL with $\lambda = 2.23$ Å. IN13 offers an energy resolution of $\delta\hbar\omega \approx 8\mu eV$ and covers a large Q-range from 0.2 to 4.9 Å^{-1}. The dry sample and hydrated samples ($n_w = 4$) with both, protonated and deuterated water, were investigated. The resolution function $R(Q, \omega)$ was determined from the measurement of a sample at 2 K. The acquired data were corrected for detector efficiency, sample container, and absorption using the standard programs available at ILL.

C. ^{2}H-NMR experiments

In solid state ^{2}H-NMR experiments, the NMR frequency in the rotating frame ω_Q is probed,[37,38]

$$\omega_Q(\theta, \phi) = \pm\delta(3\cos^2\theta - 1 - \eta\sin^2\theta\cos(2\phi)). \quad (6)$$

Here, θ and ϕ are the polar coordinates between the electric field gradient and the external static field $\vec{B}_0$, δ is the anisotropy parameter of the quadrupolar coupling tensor. Working with ^2H_2O, the quadrupolar coupling tensor value is $\delta = 2\pi \times 165$ kHz and the asymmetric parameter is small ($\eta \approx 0.1$). Equation (6) can be simplified to

$$\omega_Q(\theta, \phi) = \pm\delta(3\cos^2\theta - 1), \quad (7)$$

where θ is the angle between $\vec{B}_0$ and the direction of the O$-^2$H bond. Hence, the frequency resonance of the water molecule is determined by the orientation of the water bonds along the static field.

When the characteristic time of the motion probed is much larger than the inverse of the quadrupolar coupling frequency ($\tau \gg 2\pi/\delta = 6\ \mu$s), the powder average over the orientations of the molecules leads to a broad Pake spectrum.[39] The Pake spectrum collapses for $\tau \approx 2\pi/\delta$, and in the limit of fast motions ($\tau \ll 2\pi/\delta$) the spectrum is motionally averaged, resulting in a narrow Lorentzian line. When a broad distribution of relaxation times exists, a fraction of the population can be slower than $2\pi/\delta$ while other fraction is faster.[37] Then, the obtained lineshape is comprised between a Pake spectrum and a motionally averaged line, called two-phase spectrum.[37]

In the case of quadrupolar interaction and assuming isotropic relaxation the spin lattice relaxation time T_1 can be written as

$$\frac{1}{T_1} = \frac{2}{15}\delta^2\left[J_1(\omega_L) + 4\,J_1(2\,\omega_L)\right] \quad (8)$$

with ω_L the Larmor frequency ($\omega_L = 2\pi \times 46.08$ MHz) and $J_1(\omega)$ the spectral density of the molecular reorientation.[40] T_1 is minimum when the correlation times are resonant with the Larmor frequency ($\tau \approx 2\pi/\omega_L$)–in our case for motions around the nanosecond time scale. From a quantitative analysis of T_1 it is possible to extract relaxation times via assumption of the shape of the spectral density or the relaxation function.

All the measurements were carried out on a Bruker 300 NMR spectrometer with a magnetic field of 7.4 T corresponding to a ^{2}H NMR Larmor frequency of 46.07 MHz. A Bruker VT heating unit, working with a nitrogen flow, was used to control the sample temperature. This control leads to absolute values correct within ±1 K. Depending on the liquid- or solid-like aspect of the response, single pulse or solid echo sequences with $\pi/2$ pulse of 2.4 μs were employed. The pulse spacing for solid-echo experiments was set to 20 μs in order to exceed the approximately 12 μs receiver dead-time. For spin-lattice relaxation, the inversion recovery quadrupolar echo sequence was used.

III. RESULTS

A. Diffraction with polarization analysis

Figure 1 shows the ratio between coherent and incoherent scattering cross sections for the different samples investigated. The results of PVP/D_2O samples at the two concentrations ($n_w = 4$ and $n_w = 2$) display very similar features at high Q-values, with a clear maximum centered at about 1.75 Å^{-1}. In this region, the coherent scattering of the fully protonated

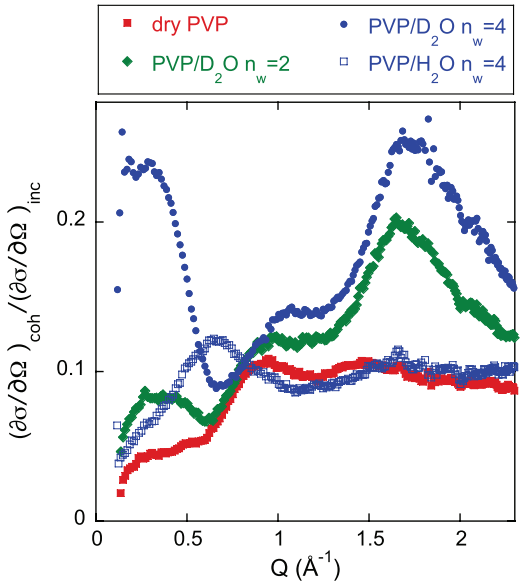

FIG. 1. Ratio between coherent and incoherent differential cross sections for the different samples investigated at RT.

This article is copyrighted as indicated in the article. Reuse of AIP content is subject to the terms at: http://scitation.aip.org/termsconditions. Downloaded to IP: 161.111.180.191 On: Fri, 05 Sep 2014 09:36:11

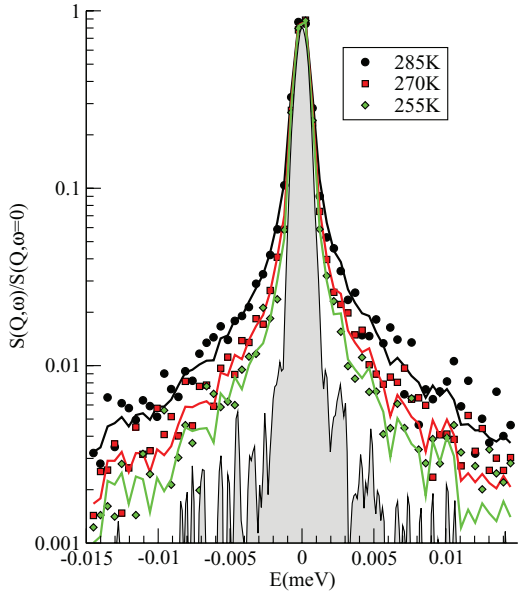

FIG. 2. Quasielastic spectra of PVP/D_2O sample ($n_w = 4$) obtained by IN16 for $Q = 1$ Å^{-1} at 285 K, 270 K, and 255 K. Symbols are experimental results, solid lines are fits using a KWW model with $\beta_{kww} = 0.35$, convoluted with the measured resolution (indicated in gray).

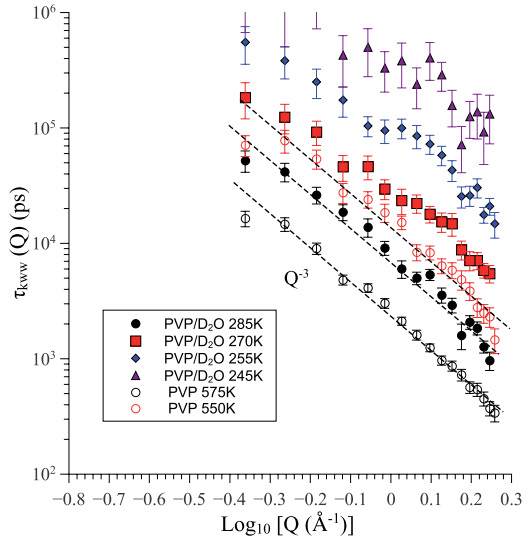

FIG. 3. Q-dependence of the relaxation times of dry PVP at 575 K (empty black circles) and 550 K (empty red circles) and PVP in PVP/D_2O solution ($n_w = 4$) at 285 K (full black circles), 270 K (full red squares), 255 K (full blue diamonds), and 245 K (full black triangles). Dashed lines show a $\tau_{kww} \propto Q^{-3}$ behavior.

hydrated sample is almost flat. Around 0.7 Å^{-1} both systems with deuterated water display a marked loss of intensity, while the PVP/H_2O sample ($n_w = 4$) shows enhanced intensity. At lower Q, the intensity of the D_2O-sample with $n_w = 4$ strongly increases, presenting a strong maximum. In this Q-region the $n_w = 2$ results also show a (much less intense) peak. The data of the dry sample, displayed as reference, present a first clear peak centered at about 0.9 Å^{-1} and a second one at about 1.5 Å^{-1}.

B. Quasielastic neutron scattering

1. PVP in deuterated water

In the PVP/D_2O ($n_w = 4$) sample, 90% of the signal measured originates from the incoherent scattering of the polymer hydrogens (see Table II and Fig. 1) and hence, for this concentration the water contribution (predominantly coherent scattering) can be safely neglected. Figure 2 shows some representative spectra at $Q = 1$ Å^{-1}. For $T \leq 225$ K the quasielastic contribution was negligible in the whole Q-range investigated.

In the Q-range and dynamic window explored by IN16, the intermediate scattering function corresponding to hydrogen motions of glass-forming polymers in the supercooled liquid state decays through a slow structural relaxation that is usually phenomenologically described by a Kohlrausch-Williams-Watts (KWW) function,

$$S(Q,t) = A(Q)\exp\left[-\left(\frac{t}{\tau_{kww}(Q)}\right)^{\beta}\right]. \quad (9)$$

Here, β is the stretching parameter accounting for the deviations from exponential behavior. It can take values between 0 and 1, and for polymers is usually of the order of 0.5.[41] $\tau_{kww}(Q)$ is the characteristic time at a given Q-value. The prefactor $A(Q)$ is an effective Lamb-Mössbauer factor that parametrizes the contribution of the fast dynamics (below some ps) to the decay of the intermediate scattering function. The experimental data have thus been fitted at each Q-value by the Fourier transform of a KWW function convoluted with the experimental resolution,

$$S_{exp}^{PVP/D_2O}(Q,\omega) = R(Q,\omega) \otimes \int_0^{+\infty} \exp(-\imath\omega t)\, A^{PVP}(Q) \times \exp\left[-\left(\frac{t}{\tau_{kww}^{PVP}(Q)}\right)^{\beta^{PVP}(Q)}\right] dt. \quad (10)$$

In a first approach, we fitted the data letting all parameters ($A^{PVP}(Q)$, $\tau_{kww}^{PVP}(Q)$, $\beta^{PVP}(Q)$) free. Since no significant and systematic Q-dependence could be determined for $\beta^{PVP}(Q)$, its value was fixed to the average (i.e., $\langle\beta^{PVP}\rangle = 0.35$) and the amplitude and relaxation times were fitted again. Such fits describe the data well as shown in Fig. 2. The Q-dependent relaxation times obtained for the different temperatures are displayed in Fig. 3. There we also show the results reported for the homopolymer at 575 K and 550 K in a previous work,[42] where the IN16 results on dry PVP were also described by Eq. (9) with the same β-value. The Q-dependence of the characteristic time of the hydrated polymer is similar to that found for the dry system. Both can be well described by a power law $\tau_{kww} \propto Q^{-3}$ in the whole Q-range investigated.

2. PVP/H_2O

Information about the dynamics of the water component can be obtained from the PVP/H_2O spectra. For this sample, the total intermediate incoherent scattering function can be

This article is copyrighted as indicated in the article. Reuse of AIP content is subject to the terms at: http://scitation.aip.org/termsconditions. Downloaded to IP: 161.111.180.191 On: Fri, 05 Sep 2014 09:36:11

expressed as

$$S_{inc}^{PVP/H_2O}(Q,t) = f_{water} S_{inc}^{water}(Q,t) + f_{PVP} S_{inc}^{PVP}(Q,t) \quad (11)$$

with f_{water} and f_{PVP} the relative scattering weights determined from the respective cross sections of each component. Hence, for a proportion of 4 water molecules/monomeric unit we obtain $f_{water} = \sigma_{water}/\sigma_{water+PVP} = 0.46$ and $f_{PVP} = \sigma_{PVP}/\sigma_{water+PVP} = 0.54$.

Due to low-frequency rotational motions of water, a decoupling between translational and rotational motions is expected.[43–45] Therefore, we restricted the analysis to Q-values lower than 1.2 Å^{-1}, where the rotational part of Sears expansion can be neglected[44,45] and the spectra should only be sensitive to translational motions. Taking into account experimental results on confined and hydration water,[45–53] and simulations of confined[54,55] and supercooled bulk water,[56] the incoherent scattering function of water hydrogens $S_{inc}^{H_2O}(Q,t)$ in this Q-range may be described as a KWW function (Eq. (9)), as it has been proposed in the relaxing cage model (see, e.g., Ref. 57).

We thus analyzed the PVP/H_2O dynamic structure factor as the sum of two stretched exponentials,

$$S^{\mathrm{PVP/H_2O}}(Q,\omega) = R(Q,\omega) \otimes \int_0^{+\infty} \exp(-\imath\omega t)\, A(Q) \times \left(f_{water} \exp\left[-\left(\frac{t}{\tau_{kww}^{water}} \right)^{\beta^{water}} \right] + f_{PVP} \exp\left[-\left(\frac{t}{\tau_{kww}^{PVP}} \right)^{\beta PVP} \right] \right) dt. \quad (12)$$

The values of the parameters β^{PVP} and τ_{kww}^{PVP} characterizing the hydrated PVP dynamics were fixed to those deduced from the analysis of the PVP/D_2O results. When the quasielastic broadening of the PVP/D_2O spectra is negligible in the IN16 window ($T \lessapprox 245$ K), the polymer contribution was considered to be elastic ($\delta(\omega)$, equivalent to $\tau_{kww}^{PVP} = \infty$).

We have assumed the prefactor $A(Q)$ to be the same for both components (as we will see below, this is justified by the EFWS results). In a first approach, the three parameters related to the dynamics of the water fraction (namely, $A(Q)$, β^{water}, and $\tau_{kww}^{water}(Q)$) were allowed to float, which results in a shape parameter β^{water} close to 0.5 in the Q-range studied–in accordance with that used in the relaxing cage model. In a second step, we fixed β_{water} to 0.5 and refined the fast decay contribution $A(Q)$ and the relaxation times $\tau_{kww}^{water}(Q)$. Fit curves following this procedure are shown in Figs. 4(a) and 4(b).

The resulting relaxation times for the water component are displayed in Fig. 5 for the different temperatures investigated. In the Q-range from 0.7 to 1.2 Å^{-1} the data can be well described by a $\tau_{kww}^{water}(Q) \propto Q^{-2}$ power law. At lower Q-values, the characteristic times seem to follow a somewhat weaker Q-dependence. We have to point out that in the low-T range explored ($T = 215$ K and 210 K) the broadening on IN16 is hardly visible, the fitted linewidths show no Q-dependence and the error becomes large.

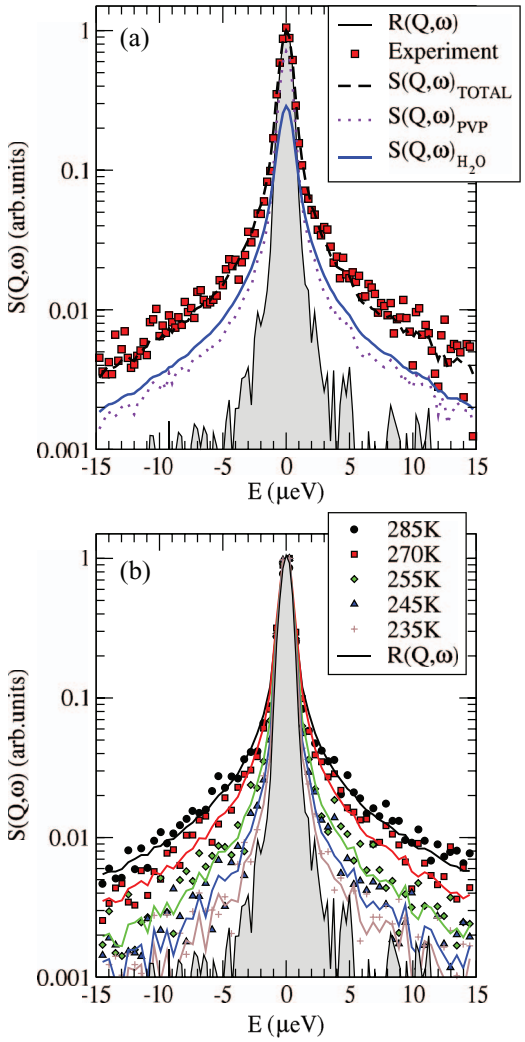

FIG. 4. Quasielastic spectra of PVP/H_2O sample ($n_w = 4$) at $Q = 1$ Å^{-1} (symbols). Resolution at 2 K is indicated in gray. (a) Results at 270 K. Black dashed line is the total fit, violet dotted line is the polymer contribution and blue solid line is the water contribution. (b) Results at 285 K, 270 K, 255 K, 245 K, and 235 K. Solid lines are fits using two KWW functions or an elastic contribution and a KWW function as described in Eq. (12).

C. Temperature-dependent EFWS

From the initial slope of the EFWS data the value of the mean squared displacement (MSD) $\langle u^2 \rangle$ can be obtained,

$$\frac{S_{inc}(Q, \omega \approx 0, T)}{S_{inc}(Q, \omega \approx 0, T \approx 0)} = I_o \exp\left(-\frac{\langle u^2 \rangle Q^2}{3} \right). \quad (13)$$

Here, the parameter I_o accounts for multiple scattering effects and normalization uncertainties.[48,58,59] It is important to notice that the MSD accessed corresponds to the slowest time resolvable by the instrumental resolution (about 0.5 ns for IN13). The explored time in these measurements is of the same order as the fastest ones accessible by IN16. In a glassy solid the extracted values of $\langle u^2 \rangle$ can be identified with the average atomic (H) displacements within the cage imposed by the neighbors. However, at high temperatures the meaning of the such obtained MSD has to be cautiously considered. When quasielastic contributions become of the same order as the instrumental resolution the $\langle u^2 \rangle$ values are affected

This article is copyrighted as indicated in the article. Reuse of AIP content is subject to the terms at: http://scitation.aip.org/termsconditions. Downloaded to IP: 161.111.180.191 On: Fri, 05 Sep 2014 09:36:11

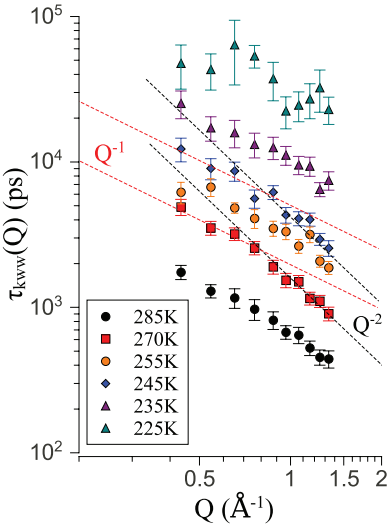

FIG. 5. Relaxation times of water in PVP/H_2O solution ($n_w = 4$) at different temperatures as function of Q. For $Q > 0.7$ Å^{-1}, the Q-dependence it is compatible with a $\tau_{kww}^{water} \propto Q^{-2}$ power law, while below it approaches a $\tau_{kww}^{water} \propto Q^{-1}$ dependence.

by them. In fact, they depend on the considered instrumental resolution. The MSD results reflect the decay of $S_{inc}(Q, t)$ through fast processes (vibrations and rapid motions) and also relaxational processes. In this sense, we may call the obtained $\langle u^2 \rangle$ "apparent" MSD. On the other hand, we emphasize that Eq. (13) implicitly assumes the Gaussian approximation, which is usually not fulfilled by glass-forming systems. Therefore, only the low-Q range $\lesssim 1$ Å^{-1} was considered to apply Eq. (13). For larger Q-values significant deviations from this equation are usually found.

The $\langle u^2 \rangle$ values obtained for the dry homopolymer are displayed in Fig. 6. This parameter increases linearly with temperature until 320 K ($\langle r^2 \rangle$(320 K) = 0.65 Å^2), in good

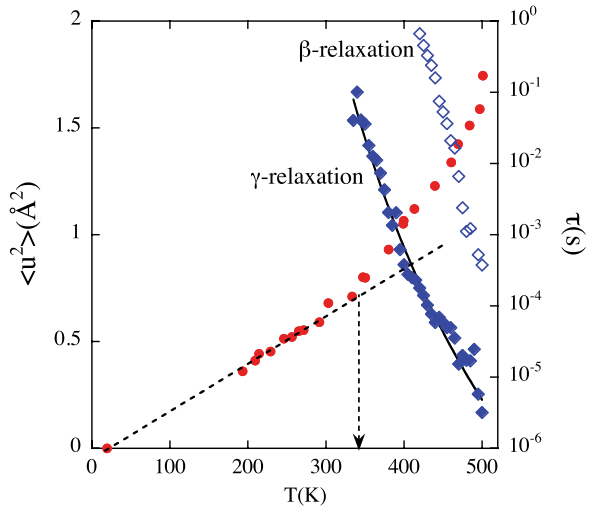

FIG. 6. Temperature dependence of the mean squared displacement (solid circles) obtained from the EFWS on dry PVP. The dashed line indicates the low-T linear dependence and the arrow marks the temperature where a change in the slope takes place. Diamonds show the characteristic times determined from BDS measurements for the γ- (solid) and β-relaxation (empty).[27] Solid line shows an Arrhenius description of the characteristic times of the γ-process with $\tau_o = 0.013$ ps and $E_a = 0.85$ eV.

agreement with a harmonic vibrational model. We note however that the values of $\langle u^2 \rangle$ in this low-T range are significantly larger than those usually reported for glass-forming homopolymers with only small (methyl) side-groups, such as poly(ethylene propylene) or head-to-head polypropylene,[60] and also containing aromatic rings such as polystyrene,[61] polycarbonate, phenoxy, and polysulfone.[62] Above 320 K an abrupt change in the slope occurs towards another linear regime where $\langle u^2 \rangle$ increases in a much steeper way, indicating that a significant number of relaxation modes are activated. The comparison with the BDS results on this polymer[27] shown in the figure suggests that the responsible for this behavior at $T \approx 320$ K would be the onset of the γ-relaxation. This process has been interpreted as the structural relaxation of the pyrrolidone rings inside the nanodomains they conform, that would be completely decoupled from the (frozen) backbone dynamics in the low temperature region.[10,42]

The same analysis on the hydrated polymer systems delivers the MSDs shown in Fig. 7(b). Considering first the results on the PVP/D_2O sample revealing hydrated PVP dynamics we observe that: (i) In the range $T \leq 250$ K, the MSD is clearly reduced as compared to the dry one, while at higher temperatures it is substantially enhanced. (ii) Below $T \approx 210$ K the MSD of wet PVP increases linearly with T (solid line in the figure), in agreement with a harmonic approximation of vibrational states. (iii) At higher temperatures, the T-dependence becomes more dramatic and can be well described by another linear regime with larger slope (dashed line). (iv) Deviations from the this second linear regime can be seen at ≈250 K.

The results on the fully hydrogenated sample also contain information on the water displacements. For the investigated composition, about 48% of the incoherent scattering is produced by the water component. Therefore, the results on the MSD of this sample reveal PVP and water contributions almost equally weighted. We observe that the MSD obtained from PVP/D_2O and PVP/H_2O samples show striking similarity. This implies that in the relatively short times probed by the elastic scans the MSDs of both, polymer and water components, behave in a very similar way. We note that this observation justifies the assumption made in the IN16 analysis of a common $A(Q)$ value for both, polymer and water fractions. Only at the highest temperatures investigated the data of the fully protonated sample seem to be systematically above those of the partially deuterated system, hinting somewhat larger displacements of the water hydrogens with respect to the polymer hydrogens.

D. NMR

To access to the spin-lattice relaxation we used the inversion recovery sequence of quadrupolar-echo. The time-dependent build-up of magnetization was described as

$$M(t) = M_0 \left(1 - 2\exp\left[-\left(\frac{t}{T_1}\right)^{\beta}\right]\right), \qquad (14)$$

where the parameter β takes into account the eventual non-exponentiality of the spin-lattice relaxation.[37] When the

This article is copyrighted as indicated in the article. Reuse of AIP content is subject to the terms at: http://scitation.aip.org/termsconditions. Downloaded to IP: 161.111.180.191 On: Fri, 05 Sep 2014 09:36:11

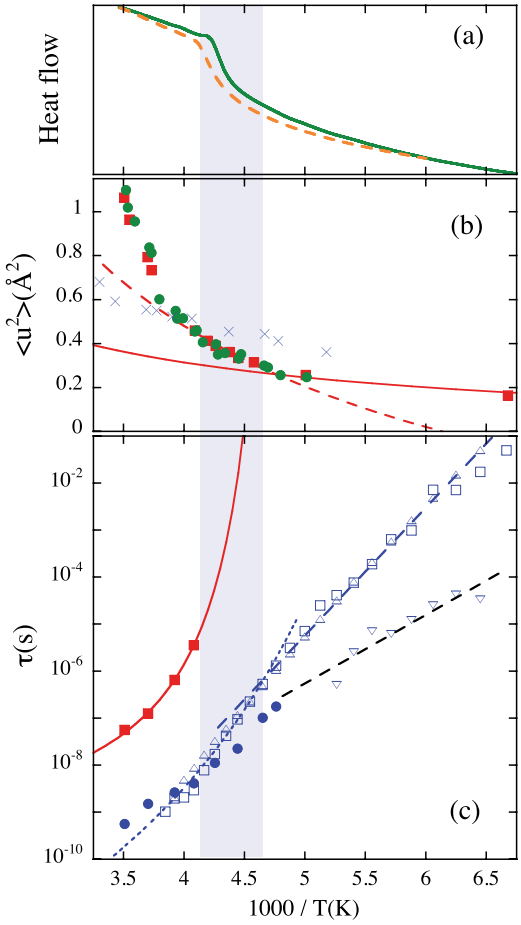

FIG. 7. Results for hydrated PVP with $n_w = 4$. (a) DSC scans of the fully protonated sample (solid, green) and the sample with deuterated water (dashed, orange). (b) Mean squared displacement obtained from the EFWSs on the PVP/D_2O (red squares) and the PVP/H_2O sample (green circles). Lines: $\langle u^2\rangle(\text{Å}^2) = -0.02625 + 0.00136 \times \text{T(K)}$ (solid) and $\langle u^2\rangle(\text{Å}^2) = -0.8999 + 0.00552 \times \text{T(K)}$ (dashed) describing the linear regimes at low and intermediate temperatures, respectively. The results on the dry PVP sample are shown as crosses for comparison. (c) Relaxation map. Red squares: average relaxation times of PVP obtained from QENS at $Q = 1$ Å^{-1}. Blue solid circles: mean relaxation times of water obtained from QENS at $Q = 1$ Å^{-1}. Triangles: Maximum of the Cole-Cole distribution of the "strong" process (BDS). Inverted triangles: Maximum of the Cole-Cole distribution of the "weak" process (BDS).[27] Empty squares: Cole-Cole relaxation times obtained from spin-lattice relaxation measurements. Lines are VF and Arrhenius fits (see text). The shadowed area shows the region of the calorimetric glass-transition.

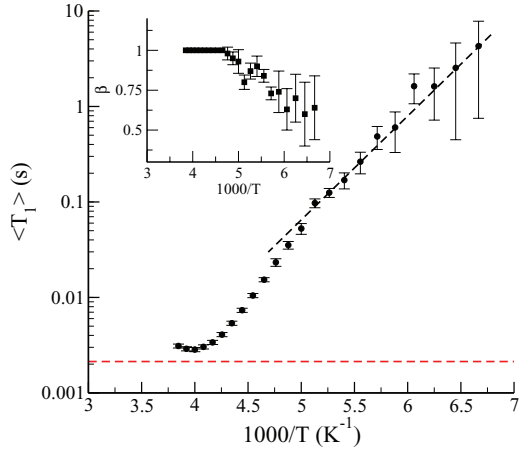

FIG. 8. Arrhenius plot of mean spin-lattice relaxation time of water $\langle T_1\rangle$. Inset: non-exponential parameter. The dashed line is the minimum of T_1 for a Debye process.

microscopic times involved in the magnetization loss are much faster than the magnetization decay time, the distribution of relaxation times is averaged during the time of the experiment, hence the magnetization build up shows an exponential behavior in time. However, if a part of the distribution of microscopic relaxation times becomes of the order of the magnetization build up time, this distribution is not fully averaged during the magnetization build up time and $M(t)$ displays a non-exponential behavior. In Fig. 8 we show the average relaxation times $\langle T_1\rangle = \Gamma(1/\beta)T_1/\beta$ and the β parameters obtained from the spin-lattice relaxation analysis. The β-values deviate from 1 at around $T \approx 200$ K, indicating that at this temperature part of the relaxation times become of the order of the spin lattice relaxation time. On the other hand, the minimum value found for T_1 (2.8 ms at around 250 K) is larger than that expected in the case of a Debye relaxation (1.3 ms, indicated by the dashed red line in Fig. 8), implying the existence of a distribution of relaxation times at high temperature. As the minimum value of T_1 is obtained when the microscopic most effective motion is in resonance with the Larmor frequency, we can conclude that at T $\approx$ 250 K the relaxation time of water motions is around $\tau_{250\,K} \approx 2\pi/\omega_L \approx$ 21.3 ns. Toward lower temperatures, T_1 increases until 200 K, where a change of the slope can be discerned.

To obtain the relaxation times we have to assume a functional form for the spectral density. The main process of confined water in the dielectric spectra could be described by a Cole-Cole distribution with an exponent $\beta_{CC} = 0.5$ roughly independent of temperature.[27] We thus assumed such a Cole-Cole spectral shape,

$$J_{CC}(\omega_L) = Im\,\frac{1}{\omega_L}\left[\frac{1}{1+\imath\,(\omega_L\tau_{CC})^{\beta_{CC}}}\right] = \frac{1}{\omega_L}\left[\frac{(\omega_L\tau_{CC})^{\beta_{CC}}\sin\left(\beta_{CC}\frac{\pi}{2}\right)}{1+2\,(\omega_L\tau_{CC})^{\beta_{CC}}\cos\left(\beta_{CC}\frac{\pi}{2}\right)+(\omega_L\tau_{CC})^{2\beta_{CC}}}\right], \quad (15)$$

and calculated the microscopic times τ_{CC} from $\langle T_1\rangle$ by means of Eq. (8). The results are plotted in Fig. 7. As can be seen, the relaxation times obtained by this procedure from the NMR experiments are in excellent agreement with those extracted from BDS for the main process.

Figure 9 shows solid-echo spectra of deuterated water in the PVP/D_2O sample at $n_w = 4$ hydration level. The lineshape progressively changes from a narrow Lorentzian at 235 K to a broad Pake pattern at 160 K. Between 225 K and 180 K two-phase spectra are found. The observation of both features is characteristic of the existence of a broad distribution of correlation times. A fraction of the water molecules have relaxation times much faster than the inverse of the quadrupolar frequency ($\tau \ll \frac{1}{\delta} \approx \mu s$), another fraction have

This article is copyrighted as indicated in the article. Reuse of AIP content is subject to the terms at: http://scitation.aip.org/termsconditions. Downloaded to IP: 161.111.180.191 On: Fri, 05 Sep 2014 09:36:11

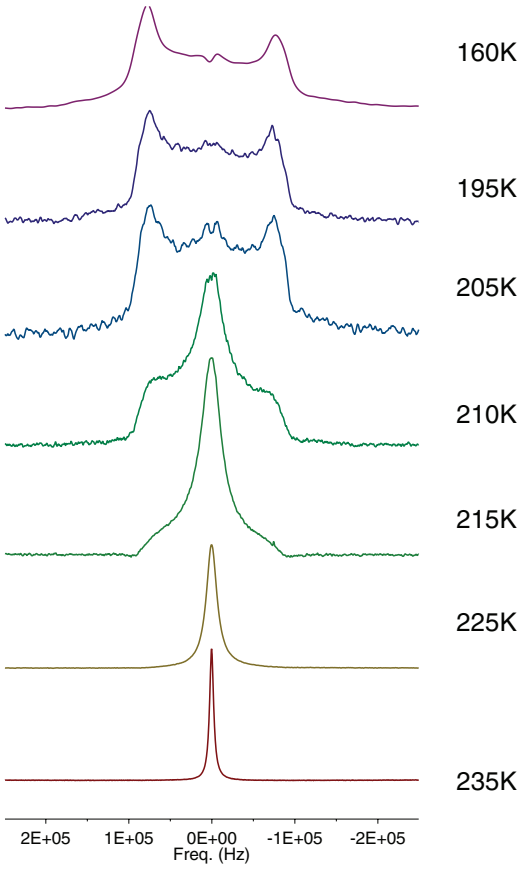

FIG. 9. ^{2}H NMR solid-echo spectra of PVP/D_2O recorded using a solid-echo delay of 20 μs.

relaxation times much slower than $\frac{1}{\delta}$, leading to an averaged and a non-averaged motion[37,63–65] in the μs time scale.

We assumed that the results between 225 K and 180 K can be described as the sum of a Lorentzian and a Pake spectrum,

$$I_{total}(\omega) = A_{Lor} I_{Lor}(\omega) + A_{Pake} I_{Pake}(\omega), \tag{16}$$

where $I_{Lor}(\omega)$ and $I_{Pake}(\omega)$ are the normalized Lorentzian and Pake contributions and A_{Lor} and A_{Pake} the respective areas. An example of such a decomposition, done using the DMFIT software,[66] is displayed in the bottom right inset of Fig. 10. The integral of each component reflects the fraction of population for which the dynamics is averaged or non averaged. Hence, we determine the fraction of "fast" molecules W_{fast} at each temperature as

$$W_{fast} = \frac{A_{Lor}}{A_{Lor} + A_{Pake}}. \tag{17}$$

The obtained values are plotted in Fig. 10. W_{fast} gradually vanishes upon cooling. Keeping in mind that the fraction of "fast molecules" reflects a temperature-dependent distribution of relaxation times $G(\ln(\tau), T)$ and employing some approximations, we can determine the width of such distribution. We assume that $G(\ln(\tau), T)$ corresponds to Arrhenius-like processes with common prefactor τ_0 and associated activation energies distributed according to a Gaussian function of width σ_E and centered around a mean value E_a. Then, $G(\ln(\tau), T)$

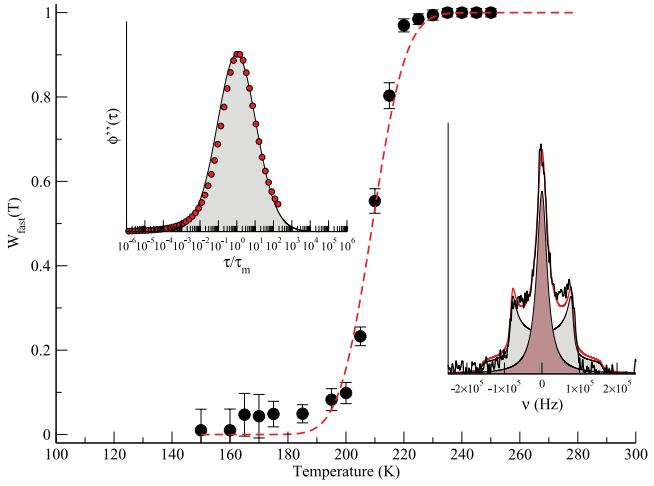

FIG. 10. Temperature dependence of the relative contribution of the Lorentzian component to the solid-echo spectrum obtained from Eqs. (16) and (17). Left inset: Loss part of a spectrum calculated using the log-normal distribution of correlation times corresponding to the parameters found with the lineshape analysis (grey area) compared with a rescaled loss dielectric spectrum at the same temperature and concentration (red points). Right inset: decomposition of the NMR pattern at 210 K in terms of Eq. (16) using DMFIT software.[66]

can be described as a log-normal distribution

$$G(\ln(\tau, T)) = \frac{1}{\sigma_{\ln(\tau)}(T)\sqrt{2\pi}} \exp\left(-\frac{\left[\ln\left(\frac{\tau}{\tau_m(T)}\right)\right]^2}{2\sigma^2_{\ln(\tau)}(T)}\right), \tag{18}$$

where the maximum τ_m can be written as $\tau_m = \tau_0 \exp(\frac{E_a}{kT})$ and the width $\sigma_{ln(\tau)}$ is given by $\sigma_{\ln(\tau)}(T) = \sigma_E/T$. As the "fraction of fast molecules" at a given temperature is related to the proportion of molecules with relaxation times smaller than the inverse of the quadrupolar echo frequency, we can write the following relation:

$$W_{fast} = \int_0^{\frac{1}{\delta}} G(\ln(\tau), T)\, d\tau. \tag{19}$$

This integral leads to the following expression:[67–69]

$$W_{fast} = \frac{1}{2}\left[1 + \mathrm{erf}\left(\frac{-\ln\left(\tau_0 \exp\left(\frac{E_a}{kT}\right)\delta\right) T}{\sigma_E\sqrt{2}}\right)\right]. \tag{20}$$

From the fit of Eq. (20) to the obtained fraction, we find a mean activation energy of $E_a = 0.42$ eV, $\sigma_E \approx 202$ K, and $\tau_0 \approx 1.3 \times 10^{-3}$ ps. Assuming that the individual events lead to Debye relaxation, the total associated relaxation spectrum is

$$\phi^*(\omega) = \int_0^{+\infty} G(\ln\tau)\left(\frac{1}{1 + \imath\omega\tau}\right)\frac{d\tau}{\tau}. \tag{21}$$

The top left inset of Fig. 10 shows the calculated loss part of the spectrum corresponding to the log-normal distribution at 202 K together with the normalized loss-part of the measured dielectric spectrum ($\epsilon''(\omega)/\epsilon''(\omega_{max})$) at 200 K.[27] The shape of the relaxation probed by BDS is in excellent agreement with that obtained via the log-normal distribution found by ^{2}H NMR lineshape decomposition.

This article is copyrighted as indicated in the article. Reuse of AIP content is subject to the terms at: http://scitation.aip.org/termsconditions. Downloaded to IP: 161.111.180.191 On: Fri, 05 Sep 2014 09:36:11

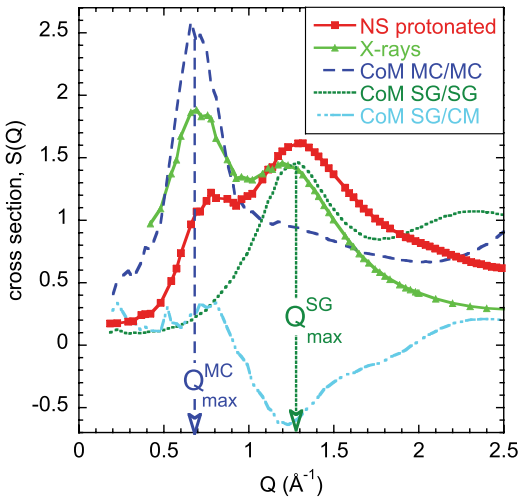

FIG. 11. Results from MD-simulations on dry PVP (Ref. 42) at 650 K. Differential cross sections accessible by x-rays (triangles) and neutron diffraction on a protonated sample (squares). Dashed and dotted lines show the static structure factor of the centers of mass of main-chains and side-groups, respectively, and dashed-dotted line represents their cross correlations. Vertical arrows mark the positions of the main peaks of the coarse-grained partial structure factors.

IV. DISCUSSION

A. Structure

Without aid of simulations, unraveling the origin of the different peaks of the diffraction patterns in complex polymeric materials is not an easy task. Though we have not simulated the hydrated system, the insight in the short-range order of dry PVP provided by molecular dynamics (MD)-simulations in an earlier work,[42] which is briefly summarized in the following, can be of utmost help to interpret the present results in the hydrated samples.

Figure 11 shows simulation results on the dry PVP protonated sample at 650 K.[42] Below 2.5 Å^{-1}, the diffraction patterns obtainable by either x-rays (XR) or NS show two clear peaks. They are located at $Q_I^{XR} = 0.7$ Å^{-1} and $Q_{II}^{XR} = 1.2$ Å^{-1} in the XR-pattern, and are slightly shifted toward higher Q-values in the case of NS ($Q_I^{NS} = 0.8$ Å^{-1} and $Q_{II}^{NS} = 1.3$ Å^{-1}). Their relative intensities also vary due to the different weighing scattering lengths. Coarse-graining the system by considering the centers of mass of the pyrrolidone ring conforming the side group (SG) and the vinyl group (MC), it was possible to calculate the associated structure factor and its contributions, eliminating non-essential ingredients. As can be seen in Fig. 11, the position of the marked main peak of the MC/MC partial structure factor Q_{max}^{MC} coincides with Q_I^{XR}. This peak could be univocally attributed to MC/MC inter-molecular correlations, revealing a prominent characteristic length in the backbone distance corresponding to $d_{MC} \approx 2\pi/Q_{max}^{MC} = 10.5$ Å–much larger than those usually found in simpler polymers. The partial structure factor involving the side-groups shows a first main peak at $Q_{max}^{SG} \approx 1.3$ Å^{-1} ($=Q_{II}^{NS}$) that contains both inter- and intra-molecular correlations and reveals a characteristic average distance between SG centers of mass $d_{SG} \approx 2\pi/Q_{max}^{SG} = 5$ Å. The strong anticorrelation peak displayed by the cross correlation term at Q_{max}^{SG} and the analysis in real space pointed to nanosegregation of MC and SGs and the existence of "ring domains." Two relevant length scales emerge as a consequence, associated to the two peaks: that corresponding to MC/MC intermolecular correlations Q_{max}^{MC} and that of SG/SG correlations Q_{max}^{SG}. It was also shown that this peculiar structure has also a strong impact on the dynamical features of PVP.[42]

In Fig. 1 the maxima of the D7 data on dry protonated PVP at RT are located at $Q_I^{NS} = 0.9$ Å^{-1} and $Q_{II}^{NS} = 1.5$ Å^{-1}, i.e., they are slightly shifted toward larger Q-values with respect to the simulation results at 650 K. This difference can be rationalized taking into account thermal expansion effects, since the experiments were performed deep in the glassy state and the simulations correspond to a temperature about 200 K above the glass-transition. Concerning the observed change in the relative intensities of the two peaks, we note that a clear decrease of the intensity of the peak dominated by the inter-molecular backbone correlations with increasing temperature has also been reported for the structure factor measured on protonated 1,4-polybutadiene.[70,105] With all, we can state that the simulations results (that were previously validated by comparison with XR measurements at high T) would also be compatible with the NS results on the protonated dry PVP sample at RT. Translating thus the interpretation of the structural information provided by the simulations to the experimental data of Fig. 1, we would deduce that the relevant length scales at RT would be determined by $Q_{max}^{SG}(RT) \approx Q_{II}^{NS} = 1.5$ Å^{-1} and $Q_{max}^{MC}(RT) \approx Q_I^{NS} - 0.1$ Å^{-1} ≈ 0.8 Å^{-1}, leading to $d_{SG} \approx 4$ Å and $d_{MC} \approx 8$ Å.

The coherent cross section of a hydrated sample contains three partial contributions composed by the correlations between pairs of atoms (i) belonging to the polymer (PVP/PVP); (ii) belonging to water molecules (water/water), and (iii) belonging to water and polymer (water/PVP), weighted by the corresponding products of neutron scattering lengths (Eq. (1)). Table III lists the relative weights of the three partial structure factors to the coherent scattering cross sections of the hydrated samples investigated, calculated considering the different scattering lengths involved and the relative abundance of the atomic pairs. The coherent cross section in the PVP/H_2O sample is mainly dominated by PVP/PVP correlations; PVP/water correlations are also relatively important, and water/water correlations are weakly weighted. If the first main peak in this pattern is attributed to PVP/PVP correlations, a relatively large shift of its position (≈0.25 Å^{-1}) with respect to that in the dry sample is inferred. Accordingly, the average inter-chain distances in PVP would increase

TABLE III. Relative weights of the different contributions to the coherent scattering in the sample defined as $f_{coh}^{A/B} = \sum_{\alpha_A \in A, \beta_B \in B} b_{\alpha_A} b_{\beta_B} / \sum_{\alpha,\beta} b_\alpha b_\beta$.

Sample	$f_{coh}^{PVP/PVP}$	$f_{coh}^{water/water}$	$f_{coh}^{water/PVP}$
PVP/D_2O ($n_w = 4$)	0.05	0.61	0.34
PVP/D_2O ($n_w = 2$)	0.13	0.41	0.46
PVP/H_2O ($n_w = 4$)	2.12	0.20	− 1.33

This article is copyrighted as indicated in the article. Reuse of AIP content is subject to the terms at: http://scitation.aip.org/termsconditions. Downloaded to IP: 161.111.180.191 On: Fri, 05 Sep 2014 09:36:11

from $d_{MC} \approx 8$ Å to about 10 Å in the presence of water. We also realize about a shoulder at ≈ 0.9 Å^{-1} that could be reminiscent of unperturbed PVP main-chain/main-chain correlations. The second (SG-related) peak almost disappears, suggesting an induced distribution of inter-rings distances in the wet sample. From the results on the fully protonated sample we could thus infer that water swells the polymer chains–at least a fraction of them–and introduces disorder within the ring nanodomains.

Since the weight of the contribution of a pair of ^{1}H atoms to the coherent cross section is much smaller than that of the corresponding deuterons, deuteration enhances the visibility of a molecular group with respect to the protonated counterpart. As a consequence, in PVP/D_2O ($n_w = 4$), the largest weight corresponds to the water/water correlations, followed by that of the cross correlations. These two contributions are similarly weighted in the sample with $n_w = 2$ D_2O. In both partially deuterated samples, the polymer contribution is very weak (see Table III). The pronounced peaks observed in the D_2O-samples at 0.2 Å^{-1} and 1.7 Å^{-1} do not exist in the protonated counterpart, and could thus be attributed to water/water correlations. In particular, the peak at low Q could be assigned to the growth of the so-called ionomer peak found in different water-containing systems.[71–74] Previously, large scale structures were found by small-angle x-ray scattering in PVP-water mixture.[8] Apparently, water clusters are formed by the addition of water. We note that this feature already appears in the sample with the lower water concentration. On the other hand, the peak at about 1.7 Å^{-1} reveals a characteristic length of about 3.7 Å and could be interpreted as a "water bulk-like" peak–the value 1.69 Å^{-1} is characteristic of low-density amorphous ice.[75] The presence of such a peak is consistent with the existence of water clusters hinted by the low-Q feature. Our results thus would support the existence of water strands or small clusters found by means of MD-simulations on PVP/H_2O (Ref. 18) (note that in that case, the water concentrations investigated were even smaller ($\leq$10%)).

The contribution of a correlation involving a hydrogen atom and another one such as C adds negatively in the case of ^{1}H and positively in the case of ^{2}H. Thus, in the samples with protonated and deuterated water the water/PVP cross correlations are oppositely weighed. This gives an additional clue to interpret the results and identify the origin of the peaks, since a maximum originated from water/PVP correlations in one sample would correspond to a minimum in the otherwise labeled system. This is the situation in the region around $Q \approx 0.7$ Å^{-1}. There, instead of the maximum observed for the H_2O-sample, a minimum is found in the case of the D_2O-sample. This suggests that the maximum at 0.7 Å^{-1} in the PVP/H_2O sample could contain (in addition to the above mentioned PVP/PVP inter-MC peak) a cross contribution which is originally negative and mirrors the PVP/PVP inter-MC peak. Water molecules and polymeric main chains would thus tend to segregate. This finding suggests a kind of nanophase separation of main chains and water domains in the sample. On the other hand, in the region $Q \approx 1.1$ Å^{-1} we also observe a kind of peak for the partially deuterated sample and a minimum for the fully deuterated sample. Such contribution could correspond to a positive cross correlation. The associated characteristic length (about 6 Å) is smaller than $d_{MC} = 10$ Å and larger than the 4 Å found for d_{SG} in the dry sample. We could tentatively assign this distance to SG/water correlations within the SG-nanodomains. In particular, we note that it is rather close to the 6.6 Å separating carbonyl oxygen atoms.[18] Therefore, this peak could correspond to correlations between PVP atoms in a side group and a water molecule forming a H-bond with the carbonyl group of a neighboring ring. This would also support the finding in Ref. 18 that almost all available water molecules are in close contact with PVP carbonyl groups in the 10% water concentration sample. In principle, we would not expect the position of this contribution to change with water concentration, but its relative contribution to the intensity would increase with increasing water content. Such an increase would be the responsible of the apparent shift of the global peak toward higher Q-values from the case $n_w = 2$ to $n_w = 4$. To corroborate our interpretation of the patterns and unambiguously elucidate the detailed origin of all these peaks, the information of properly validated fully atomistic MD-simulations of hydrated samples would be crucial.

B. Dynamics

1. Dynamics of hydrated PVP

Neutron scattering selectivity has allowed isolating hydrated PVP dynamics. The EFWS study has revealed an important reduction of the polymer mobility at short times (initial decay of the intermediate scattering function) as compared with the dry sample (see Fig. 7(b)) for $T \lesssim 250$ K. The coincidence of the MSD of both, polymer and water components in this temperature range (visible in the same figure), could suggest an important role of H-bonding on the dynamics at such local length- and fast time-scales. We note however that the observed "stiffening" effect on the polymer upon inclusion of additives has recently been reported from MD-simulations of a Lennard-Jones (LJ) polymer melt with LJ-monomers as additives.[76] The fact that this effect arises in such coarse-grained simulations would imply that in the real systems it could be not only a consequence of the formation of H-bonds between polymer atoms and water. Densification of the hydrated system reducing the size of the effective cage for the atomic displacements seems to play a major role in determining the fast dynamics in the low temperature range. On the other hand, the strong plasticization induced by water (reduction of the T_g of the system by more than 200 K) leads to larger displacements of the wet polymer with respect to the dry state above 250 K.

This drastic plasticization is the only apparent effect of water on the polymer dynamics addressed by IN16, speeding up the motions–the relaxation times probed are in the nanosecond scale for temperatures differing by 300 K for hydrated and dry samples. Figure 7(c) shows the temperature dependence of the characteristic times of hydrated PVP at $Q = 1$ Å^{-1}. We have chosen this value because it is usually found that results from relaxation techniques such as BDS match QENS data at about this Q-value.[77] The hydrated PVP characteristic times follow a clear non-Arrhenius

This article is copyrighted as indicated in the article. Reuse of AIP content is subject to the terms at: http://scitation.aip.org/termsconditions. Downloaded to IP: 161.111.180.191 On: Fri, 05 Sep 2014 09:36:11

T-dependence that can be well described by means of a Vogel-Fulcher (VF) law,

$$\tau(T) = \tau_o \exp\left(\frac{B}{T - T_o}\right), \tag{22}$$

with $\tau_o = 580$ ps, $B = 359$ K, and $T_o = 204$ K. From this description the value of the "dynamic" glass-transition temperature associated to this component, defined as the temperature at which the characteristic time reaches the value of 100 s, is deduced to be 218 K. This temperature–more than 200 K below the glass-transition of dry PVP–is located in the region of the broad calorimetric glass-transition of the PVP/water system (Fig. 7(a)). We can thus say that, within the uncertainties in the extrapolation of the characteristic time, the differential scanning calorimetry (DSC) results reflect the freezing of the majority (polymeric) component. This is an interesting result because the dynamics of the PVP component cannot be followed by BDS.

No modifications can be seen in the Q-dependence and stretching of the intermediate scattering function when the polymer is hydrated. We note however that the behavior found for both, dry, and hydrated polymers, is unusual for regular glass-forming polymers. First, the value of the shape parameter used ($\beta = 0.35$) is markedly lower than that usually obtained ($\beta \approx 0.5$ (Ref. 41)), indicating extreme stretching of the intermediate scattering function. Second, the crossover in the Q-dependence of the relaxation times that is usually found reflecting a transition toward a Gaussian regime at long time and large length scales[78–88] is absent in these samples. We recall that in the dry sample the observed anomalies in the H-motions were mainly attributed to the heterogeneous dynamics undergone by MC and SG populations.

After a recent QENS work on poly(vinyl methyl ether) (PVME) concentrated aqueous solutions,[89] the expected influence of water on the polymer (in addition to the plasticization effect) is twofold: (i) to produce heterogeneous environments that translate into anomalously stretched functional forms, but do not necessarily affect the Q-dependence of the characteristic times and (ii) to hinder the motions of the molecular groups participating in the H-bonds with water, resulting in a more continuous-like diffusive motions of the involved hydrogens. This can lead to a persisting $\tau_{kww}(Q) \propto Q^{-n}$-dependence over the entire BS-window, as it has been found for PVME.[89] In hydrated PVP we also observe all these expected features. The particularity in this case is that even in the dry system, due to its peculiar structure, strong dynamic heterogeneities and consequently anomalous Q-dependencies are already present.

2. Water dynamics

^{2}H NMR probes the reorientation of the O–D bond in water, thus being mostly sensitive to the rotational motions of this molecule. Therefore, the results obtained can be directly compared with those from BDS.[90] Neutron scattering addresses the self-correlation function of hydrogen atoms, that includes both, translational and rotational degrees of freedom. All these contributions are present in the MSDs obtained from the EFWS investigation. In the case of the IN16 study, restricting the analysis to Q-values smaller than 1.2 Å^{-1}, we mainly probe the translational component of water dynamics.

The NMR analysis above 220 K reveals a purely Lorentzian line shape, implying isotropic rotational motions faster than $\frac{1}{\delta}$. The continuous variation in the line shape toward lower temperatures could be explained with two distinct interpretations. The first one is a progressive change of the nature of the motions from isotropic to anisotropic reorientations.[63] This scenario can be discarded because then the central part of the spectrum would sensibly differ from a Lorentzian shape, which is not our case. The second explanation–and most plausible here–is a continuous slowing down of the average times of the underlying distribution of isotropic reorientation processes. With a simple model based on a distribution of reorientation times assumed as isotropic, we are also able to reproduce the width of the spectral density obtained by BDS (see Fig. 10). Using the functional form issued from BDS experiments (Cole-Cole with $\beta_{CC} = 0.5$) the characteristic times obtained from the $\langle T_1 \rangle$ relaxation experiments nicely coincide with those reported from BDS measurements for the slower process detected (see Fig. 7(c)). The combined set of characteristic times for water dynamics in the high temperature range shows a curvature, hence pointing to a cooperative-like nature of the motions. A VF law with $\tau_o = 0.01$ ps, $B = 1524$ K, and $T_o = 130$ K describes well the relaxation data in this range. At ≈ 215 K a crossover toward an Arrhenius-like behavior ($\tau_o = 1.4\text{e-}7$ ps, $E_a = 0.54$ eV) at lower temperatures is found (see Figs. 7(c)). This crossover has also been observed in different hydrophilic mixtures and dynamically asymmetric mixtures with BDS (Refs. 27, 28, and 90–92) and by ^{2}H NMR spectroscopy on different protein water systems.[63–65] The value of the activation energy $E_a \approx 0.5$ eV seems to be rather universal for these systems.

Peculiarities in the dynamical behavior in this temperature range close to 220 K are commonly found in the field on hydration studies. We note that around 210 K we also observe the first crossover in the temperature dependence of the MSD monitored by the EFWS (Fig. 7(b)). In proteins, this phenomenon is known as the dynamical transition. The nature of this transition is highly debated and its meaning is not unanimously accepted (see, e.g., Refs. 48, 50, and 93).

We now discuss the information provided by QENS mostly sensitive to the translational modes. In the high-T range (225 K $< T$) the characteristic times deduced for water dynamics from QENS at $Q = 1$ Å^{-1} overlap well with those obtained from BDS and NMR (see Fig. 7(c)). Thus, the usually observed coincidence of relaxational results with scattering results at Q-values of this order[77] is also found for the water component in this system. As previously mentioned, at lower temperatures the QENS results are subjected to large uncertainties. If we consider these data, they do not show a clear "fragile-strong" crossover and tend to smaller values than the BDS (slow) and NMR results, approaching rather the results obtained by BDS for the weak fast process. A similar situation has been found in the QENS work on PVME aqueous solutions.[89] In that work, the dielectric fast relaxation process of water could be identified with water motions coupled with PVME local relaxations, since the process coincides

This article is copyrighted as indicated in the article. Reuse of AIP content is subject to the terms at: http://scitation.aip.org/termsconditions. Downloaded to IP: 161.111.180.191 On: Fri, 05 Sep 2014 09:36:11

with the β-relaxation in dry PVME. In the case of PVP, all the relaxations of the dry polymer–at least those detectable by BDS–occur at much higher temperatures (see Fig. 6). On the other hand, Swenson *et al.*[94] have interpreted the fast process observed by BDS in several systems containing confined water as motion of Bjerrum-type defects. Though the activation energy of the fast process found in PVP/H_2O is close to that exhibited by those relaxations, the absolute values are about 30× smaller, preventing an equalization of both processes.

The stretching observed ($\beta^{water} = 0.5$) rules out simple diffusion ($\beta^{water} = 1$) of water molecules. Nevertheless, the Q-dependence of the characteristic times found in the Q-range $0.7 \leq Q \leq 1.2$ Å^{-1} is consistent $\tau_{kww}^{water} \propto Q^{-2}$–that corresponding to simple diffusion. Such simultaneous observation of stretching and Q^{-2}-dependence of the characteristic times can be interpreted as diffusive motions in heterogeneous environments.[80] Structural heterogeneities and/or concentration fluctuations would give rise to a distribution of mobilities (diffusion coefficients) leading to the observation of stretched scattering functions. We note that the existence of a distribution of relaxation times for water dynamics has been demonstrated by our NMR results on the lineshape, at least in the temperature range 180 K $\lesssim$ 220 K. On the other hand, at each temperature hints for a change in the Q-dependence of $\tau_{water}(Q)$ behavior from $Q^{-2} \rightarrow Q^{-1}$ can be envisaged at around 0.7 Å^{-1}. Having used a β-value of 0.5 to describe the stretching of the scattering function, both Q^{-2} and Q^{-1} dependencies of the characteristic time imply clear deviations from Gaussian behavior. However, the Q^{-1} power law found below 0.7 Å^{-1} is incompatible with a free diffusion model, which would imply a $\tau(Q) \propto Q^{-2}$ dependence.[44,45,52] Transitions in the Q-dependence of the characteristic time can appear in the case of spatially restricted diffusive-like motions. As an example, the model of diffusion in an impermeable sphere of radius R predicts a change in the behavior from $\tau(Q) \propto Q^{-2} \rightarrow$ constant τ when a Q value $Q \approx 2\pi/R$ is reached.[95] In our case, the change in the Q-dependence takes place at around 0.7 Å^{-1}, where the coherent cross-section of PVP/H_2O displays a maximum (respectively, PVP/D_2O shows a minimum). We have interpreted the associated length scale as that characteristic for the inter-MC correlations and the PVP/water anticorrelations. Hence, it is tempting to relate the anomalously diffusive motions appearing at low Q to the existence of nanophases in the mixture. We note that in hydrated polymer nafion, nanophase separation appears[71,73,96] and heavily affects the local relaxation and the diffusion of water molecules.[97] In the latter reference, the QENS model used in the data analysis is an extension of the diffusion in an impermeable sphere model to a semi permeable sphere, that assumes the existence of restricted motions followed by long range diffusion. Given the structural evidences for the existence of water clusters and nanosegregation in our sample, we could attribute the observed Q-dependence of the relaxation time of water molecules to the following scenario: in water-rich domains, the relaxation of water would follow a diffusive-like process, giving rise to the Q^{-2} behavior. Toward larger distances, hence to escape from a rich-water domain structure, motions would take place along pathways between water clusters, where water molecules would follow a kind of anomalous motion, probably subdiffusive, giving rise to a weaker Q-dependence of the characteristic time. Similarly, two types of water motion in a glassy PVP matrix were proposed in Ref. 17 for small water concentrations: (i) entrapment within fluidic microdomains surrounded by frozen matrix and (ii) hopping between microdomains.

Finally, we have mentioned above that the characteristic times obtained for water in the low T-range hardly depend on Q. This would be an argument for a local motion process below ≈225 K if we consider the analysis as reliable.

3. Polymer versus water dynamics: Dynamic asymmetry

As shown in Fig. 7(c), the characteristic times deduced for water from QENS experiments are much faster than those observed for the polymer component. We note that these times characterize the final slow decay of the intermediate scattering function of hydrogens, i.e., are related with the structural relaxations of the components. The dynamic asymmetry in the system Δ, defined as the ratio between the characteristic times of the slow and fast component, $\Delta = \tau^{PVP}/\tau^{water}$, increases with decreasing temperature (at $Q = 1$ Å^{-1}, $\Delta(285\text{ K}) = 50$, $\Delta(245\text{ K}) = 500$). As mentioned above, the global glass-transition–associated to the polymer component as deduced from the QENS results–occurs at around 220 K. The initial linear regime of the mean squared displacements and the Arrhenius regime in the water dynamics take place when the PVP component becomes a completely frozen matrix. Then, water can only undergo the local relaxations detectable by NMR and BDS. We can also see that the glass-transition of the system is very broad, extending over about 20 K (shadowed area in Fig. 7). In this region, the structural relaxation of the polymer component is effectively frozen with respect to the water component. Nevertheless, locally, the atomic displacements of water and polymer hydrogens at times of the order of 0.5 ns are of the same order, as inferred from their (possibly apparent, as pointed above) MSDs (Fig. 7(b)). Seemingly, there is a softening of the structure that allows larger atomic displacements at short times than those permitted in the deep glassy state. At ≈ 245 K the segmental polymer dynamics is fast enough to give rise to quasielastic broadening in the IN16 window (lowest-T reported characteristic time in Fig. 7(c)) and starts to contribute to the decay of the intermediate scattering function at about 0.5 ns. Consequently, it is detected by the EFWS and produces the second change in the slope of the (apparent) MSD at ≈ 250 K. This "crossover" thus would not be caused by any new relaxation mechanism or a real change in the dynamics and consequently it would not be expected to be noticed in the NMR or BDS experiments, as it is the case. We also note that even in the range $T \gtrsim 250$ K the values of the MSDs of water and polymer components at the short time explored by the IN13 resolution are quite similar. Water seems to be only slightly more mobile giving rise to a slight increase of the MDS in the fully protonated sample with respect to that in the sample with deuterated water. Thus, the dynamic asymmetry in the system applies only for the slow dynamics. On the contrary, the fast dynamical processes of

This article is copyrighted as indicated in the article. Reuse of AIP content is subject to the terms at: http://scitation.aip.org/termsconditions. Downloaded to IP: 161.111.180.191 On: Fri, 05 Sep 2014 09:36:11

both components seem to be highly coupled, probably via the formation of H-bonds.

The observed dynamic asymmetry for the structural relaxation of the two subsystems might be a key factor in the development of the peculiar features of water dynamics, since it provides a source for local confinement of the water molecules in the nanosegregated structure. For instance, we note the emergence of subdiffusive-like behavior for the fast particles in simulated mixtures of dynamically asymmetric components.[98–101] In real systems like polymer blends,[102,103] this dynamic asymmetry has been invoked as responsible for deviations in the temperature dependence of the relaxation time of the fast component from VF toward Arrhenius-like– in a similar way as observed for water from NMR and BDS studies. Such an interpretation was also proposed for water in PVP in the previous BDS work.[27] The NS investigation here reported provides the experimental evidence for the freezing of the PVP component in the crossover temperature range, supporting this scenario.

Finally, we comment on the comparison of our results with those obtained on other concentrated aqueous polymer solutions by applying a similar methodology, namely, PVME[89] and polyamides[104] solutions. Stretching of the intermediate scattering function and Q^{-2}-dependence of the characteristic time of water were analogously observed in those systems. Thus, the heterogeneous character of water diffusion seems to be a general feature, independently of being in environments with only H-bond acceptor sites-such as PVME and PVP–or with both donor/acceptor sites–like polyamides. Regarding the non-Arrhenius to Arrhenius crossover, it occurs in all systems and seems to be associated to the freezing of the α-relaxation of the polymer in the case of both H-bond acceptor polymers. In the case of polyamides, it was observed that the crossover in the water dynamics takes place when its characteristic relaxation times reach the values of the γ-relaxation of the polymer. This could suggest that in such donor/acceptor systems, the local mobility of the polymer could play an important role in the origin of this crossover. It is worth noting nevertheless that the concentration of water in polyamides was about 16 wt. %, i.e., much lower than in this work and in the PVME solution (30 wt. %). This difference could also be decisive in determining such a distinct behavior.

V. CONCLUSIONS

Using neutron scattering with H/D substitution labeling we have selectively studied the structure and dynamics of the polymer and water components in the PVP/H_2O system, revealing the following main observations:

(1) Swelling of the polymer chains and disorder within the ring nanodomains induced by the presence of water.
(2) Evidences for clusters of water due to nanosegregation of water and polymer main chains.
(3) Strong coupling of the fast (below $\approx$ 0.5 ns) dynamics corresponding to both components, polymer and water.
(4) Stretched exponential structural relaxation and non-Gaussian behavior of both components.
(5) Strong dynamic asymmetry between the structural relaxations of the components ($\Delta \approx 50$ at high T), that increases with decreasing temperature. We emphasize that PVP slowing down has been isolated and monitored by QENS and is compatible with the DSC observation.

NMR and BDS experiments focusing on the water component give us other indications:

(6) At $T \approx 220$ K the process observed by NMR, which coincides with the "slow" one detected by BDS, undergoes a transition from Arrhenius-like at low temperatures to VF at high temperatures.
(7) There exists a distribution of relaxation times, at least for the sub-T_g process. This is symmetric.
(8) No trace of anisotropic motions is present in the NMR spectra.

Comparing neutron scattering and relaxation results we find that

(9) The characteristic times obtained by neutron scattering at low temperatures deviate toward the "fast-process" observed by BDS. The latter has similar activation energy as the motion of Bjerrum-type defects but is much slower than in other systems.

Based on these results and trying to rationalize them we propose the following three key ingredients in this system: (i) heterogeneous structure leading to distributions of mobilities; (ii) H-bond formation and densification producing the strong coupling of the component dynamics at short times and low temperatures, and (iii) dynamic asymmetry in the slow relaxations, inducing confinement effects expressed as, e.g., a change in the relaxation process of water from a collective to a localized motion and probably anomalous Q-dependences of the characteristic times.

ACKNOWLEDGMENTS

Financial support from the projects MAT2007-63681 and IT-436-07 (G.V.) is acknowledged.

[1] V. Bühler, in *Polyvinylpyrrolidone Excipients for Pharmaceuticals* (Springer, Berlin, 2005), pp. 5–124.
[2] V. Bühler, in *Polyvinylpyrrolidone Excipients for Pharmaceuticals* (Springer, Berlin, 2005), pp. 221–225.
[3] J. Guo, G. Skinner, W. Harcum, and P. P. E. Barnum, Pharm. Sci. Technol. Today **1**, 254 (1998).
[4] B. Nair, Int. J. Toxicol. **17**, 95 (1998).
[5] N. Shinyashiki, N. Asaka, S. Mashimo, and S. Yagihara, J. Chem. Phys. **93**, 760 (1990).
[6] T. Sun and H. E. King, Macromolecules **29**, 3175 (1996).
[7] D. Sen, S. Mazumder, P. Sengupta, A. K. Ghosh, and V. Ramachandhran, J. Macromol. Sci., Phys. **39**, 235 (2000).
[8] J. van der Elsken, W. Bras, and J. Michielsen, J. Appl. Crystallogr. **34**, 62 (2001).
[9] S. Barker, R. He, and D. Craig, J. Pharm. Sci. **90**, 157 (2001).
[10] L. V. Karabanova, G. Boiteux, O. Gain, G. Seytre, L. M. Sergeeva, and E. D. Lutsyk, J. Appl. Polym. Sci. **80**, 852 (2001).
[11] C. Lau and Y. Mi, Polymer **43**, 823 (2002).
[12] M. de Dood, J. Kalkman, C. Strohhofer, J. Michielsen, and J. van der Elsken, J. Phys. Chem. B **107**, 5906 (2003).
[13] S. Kim, S. Park, K. An, N. Kim, and S. Kim, J. Appl. Polym. Sci. **89**, 24 (2003).
[14] R. J. Sengwa, Abhilasha, and N. M. More, Polymer **44**, 2577 (2003).

This article is copyrighted as indicated in the article. Reuse of AIP content is subject to the terms at: http://scitation.aip.org/termsconditions. Downloaded to IP: 161.111.180.191 On: Fri, 05 Sep 2014 09:36:11

[15]L. V. Karabanova, G. Boiteux, O. Gain, G. Seytre, L. M. Sergeeva, E. D. Lutsyk, and P. A. Bondarenko, J. Appl. Polym. Sci. **90**, 1191 (2003).
[16]S. Yagihara, M. Asano, M. Kosuge, S. Tsubotani, and N. Shinyashiki, J. Non-Cryst. Solids **351**, 2629 (2005).
[17]T.-X. Xiang and B. Anderson, J. Pharm. Sci. **93**, 855 (2004).
[18]T.-X. Xiang and B. Anderson, Pharm. Res. **8**, 1205 (2005).
[19]H. Shirota and E. W. Castner, J. Chem. Phys. **125**, 034904 (2006).
[20]N. Shinyashiki, R. J. Sengwa, S. Tsubotani, H. Nakamura, S. Sudo, and S. Yagihara, J. Phys. Chem. A **110**, 4953 (2006).
[21]N. Shinyashiki, D. Imoto, and S. Yagihara, J. Phys. Chem. B **111**, 2181 (2007).
[22]A.-V. Sarode and A.-C. Kumbharkhane, Polym. Int. **61**, 609 (2012).
[23]R. Sengwa and S. Sankhla, J. Macromol. Sci., Phys. **46**, 717 (2007).
[24]E. Tarassova, V. Aseyev, A. Filippov, and H. Tenhu, Polymer **48**, 4503 (2007).
[25]B. Vasheghani, F. Rajabi, and M. Ahmadi, Polym. Bull. **58**, 553 (2007).
[26]B. Fortier-McGill, V. Toader, and L. Reven, Macromolecules **44**, 2755 (2011).
[27]S. Cerveny, A. Alegría, and J. Colmenero, J. Chem. Phys. **128**, 044901 (2008).
[28]S. Cerveny, A. Alegría, and J. Colmenero, Phys. Rev. E **77**, 031803 (2008).
[29]R. M. Moon, T. Riste, and W. C. Koehler, Phys. Rev. **181**, 920 (1969).
[30]O. Schärpf, Physica B **182**, 376 (1992).
[31]J. Eilhard, A. Zirkel, W. Tschöp, O. Hahn, K. Kremer, O. Schärpf, D. Richter, and U. Buchenau, J. Chem. Phys. **110**, 1819 (1999).
[32]G. Meier, U. Pawelzik, W. Schweika, and W. Kockelmann, Physica B **276–278**, 369 (2000).
[33]A. M. Gaspar, S. Busch, M.-S. Appavou, W. Haeussler, R. Georgii, Y. Su, and W. Doster, Biochim. Biophys. Acta **1804**, 76 (2010).
[34]J. R. Stewart, P. P. Deen, K. H. Andersen, H. Schober, J.-F. Barthélémy, J. M. Hillier, A. P. Murani, T. Hayes, and B. Lindenau, J. Appl. Crystallogr. **42**, 69 (2009).
[35]B. Alefeld, M. Birr, and A. Heidemann, Naturwiss. **56**, 410 (1969).
[36]B. Frick and M. González, Physica B **301**, 8 (2001).
[37]R. Böhmer, G. Diezemann, G. Hinze, and E. Rössler, Prog. Nucl. Magn. Reson. Spectrosc. **39**, 191 (2001).
[38]K. Schmidt-Rohr and H. W. Spiess, in *Multidimensional Solid-State NMR and Polymers* (Academic, 1994), Vol. 496.
[39]G. E. Pake, J. Chem. Phys. **16**, 327 (1948).
[40]N. Bloembergen, E. M. Purcell, and R. V. Pound, Phys. Rev. **73**, 679 (1948).
[41]D. Richter, M. Monkenbusch, A. Arbe, and J. Colmenero, in *Advances in Polymer Science* (Springer-Verlag, Berlin, 2005), Vol. 174.
[42]R. Busselez, A. Arbe, F. Alvarez, J. Colmenero, and B. Frick, J. Chem. Phys. **134**, 054904 (2011).
[43]V. F. Sears, Can. J. Phys. **44**, 1299 (1966).
[44]J. Teixeira, M.-C. Bellissent-Funel, S. H. Chen, and A. J. Dianoux, Phys. Rev. A **31**, 1913 (1985).
[45]J.-M. Zanotti, M.-C. Bellissent-Funel, and S.-H. Chen, Phys. Rev. E **59**, 3084 (1999).
[46]R. Bergman and J. Swenson, Nature (London) **403**, 283 (2000).
[47]S.-H. Chen, L. Liu, E. Fratini, P. Baglioni, A. Faraone, and E. Mamontov, Proc. Natl. Acad. Sci. U.S.A. **103**, 9012 (2006).
[48]W. Doster, S. Busch, A. M. Gaspar, M.-S. Appavou, J. Wuttke, and H. Scheer, Phys. Rev. Lett. **104**, 098101 (2010).
[49]J. Swenson, R. Bergman, and S. Longeville, J. Chem. Phys. **115**, 11299 (2001).
[50]S. Khodadadi, S. Pawlus, J. H. Roh, V. G. Sakai, E. Mamontov, and A. P. Sokolov, J. Chem. Phys. **128**, 195106 (2008).
[51]M.-C. Bellissent-Funel, in *Soft Matter Under Exogenic Impacts*, NATO Science Series II: Mathematics, Physics and Chemistry Vol. 242, edited by S. J. Rzoska, and V. A. Mazur (Springer, Netherlands, 2007), pp. 413–431.
[52]M.-C. Bellissent-Funel, Eur. Phys. J. E **12**, 83 (2003).
[53]S. Dellerue and M. C. Bellissent-Funel, Chem. Phys. **258**, 315 (2000).
[54]P. Gallo, M. Rovere, and E. Spohr, J. Chem. Phys. **113**, 11324 (2000).
[55]P. Gallo, M. Rovere, M. A. Ricci, C. Hartnig, and E. Spohr, Europhys. Lett. **49**, 183 (2000).
[56]D. Paschek and A. Geiger, J. Phys. Chem. B **103**, 4139 (1999).
[57]S.-H. Chen, P. Gallo, F. Sciortino, and P. Tartaglia, Phys. Rev. E **56**, 4231 (1997).
[58]R. Zorn, Phys. Rev. B **55**, 6249 (1997).
[59]W. Doster and M. Settles, Biochim. Biophys. Acta **1749**, 173 (2005).
[60]R. Pérez Aparicio, A. Arbe, J. Colmenero, B. Frick, L. Willner, D. Richter, and L. J. Fetters, Macromolecules **39**, 1060 (2006).
[61]S. Arrese-Igor, A. Arbe, B. Frick, and J. Colmenero, Macromolecules **44**, 3161 (2011).
[62]S. Arrese-Igor, I. Quintana, A. Arbe, J. Colmenero, A. Alegrìa, B. Frick, and S. Janssen, Physica B **350**, e971 (2004).
[63]S. A. Lusceac, M. R. Vogel, and C. R. Herbers, Biochim. Biophys. Acta **1804**, 41 (2010).
[64]M. Vogel, Phys. Rev. Lett. **101**, 225701 (2008).
[65]C.-R. Herbers, D. Sauer, and M. Vogel, J. Chem. Phys. **136**, 124511 (2012).
[66]D. Massiot, F. Fayon, M. Capron, I. King, S. Le Calvé, B. Alonso, J.-O. Durand, B. Bujoli, and G. Hoatson, Magn. Reson. Chem. **40**, 70 (2002).
[67]E. Rössler, M. Taupitz, K. Böhmer, M. Schulz, and H.-M. Vieth, J. Chem. Phys. **92**, 5847 (1990).
[68]S. Schildmann, A. Nowaczyk, B. Geil, C. Gainaru, and R. Böhmer, J. Chem. Phys. **130**, 104505 (2009).
[69]S. A. Lusceac, M. Rosenstihl, M. Vogel, C. Gainaru, A. Fillmer, and R. Böhmer, J. Non-Cryst. Solids **357**, 655 (2011).
[70]A. Narros, A. Arbe, F. Alvarez, J. Colmenero, R. Zorn, W. Schweika, and D. Richter, Macromolecules **38**, 9847 (2005).
[71]K. Schmidt-Rohr and Q. Chen, Nature Mater. **7**, 75 (2008).
[72]G. Gebel and O. Diat, Fuel Cells **5**, 261 (2005).
[73]M.-H. Kim, C. J. Glinka, S. A. Grot, and W. G. Grot, Macromolecules **39**, 4775 (2006).
[74]G. Gebel and R. B. Moore, Macromolecules **33**, 4850 (2000).
[75]M. Bellissent-Funel, J. Teixeira, and L. Bosio, J. Chem. Phys. **87**, 2231 (1987).
[76]D. Simmons and J. Douglas, Soft Matter **7**, 11010 (2011).
[77]J. Colmenero, A. Arbe, and A. Alegría, J. Non-Cryst. Solids **172–174**, 126 (1994).
[78]A. Arbe, J. Colmenero, F. Alvarez, M. Monkenbusch, D. Richter, B. Farago, and B. Frick, Phys. Rev. Lett. **89**, 245701 (2002).
[79]A. Arbe, J. Colmenero, F. Alvarez, M. Monkenbusch, D. Richter, B. Farago, and B. Frick, Phys. Rev. E **67**, 051802 (2003).
[80]A. Arbe, J. Colmenero, M. Monkenbusch, and D. Richter, Phys. Rev. Lett. **81**, 590 (1998).
[81]J. Colmenero, F. Alvarez, and A. Arbe, Phys. Rev. E **65**, 041804 (2002).
[82]J. Colmenero, A. Arbe, F. Alvarez, M. Monkenbusch, D. Richter, B. Farago, and B. Frick, J. Phys.: Condens. Matter **15**, S1127 (2003).
[83]A. Narros, F. Alvarez, A. Arbe, J. Colmenero, D. Richter, and B. Farago, J. Chem. Phys. **121**, 3282 (2004).
[84]J. Sacristan, F. Alvarez, and J. Colmenero, Europhys. Lett. **80**, 38001 (2007).
[85]R. Pérez-Aparicio, A. Arbe, F. Alvarez, J. Colmenero, and L. Willner, Macromolecules **42**, 8271 (2009).
[86]B. Farago, A. Arbe, J. Colmenero, R. Faust, U. Buchenau, and D. Richter, Phys. Rev. E **65**, 051803 (2002).
[87]M. Tyagi, A. Arbe, J. Colmenero, B. Frick, and J. R. Stewart, Macromolecules **39**, 3007 (2006).
[88]M. Tyagi, A. Arbe, F. Alvarez, J. Colmenero, and M. A. González, J. Chem. Phys. **129**, 224903 (2008).
[89]S. Capponi, A. Arbe, S. Cerveny, R. Busselez, B. Frick, J. Embs, and J. Colmenero, J. Chem. Phys. **134**, 204906 (2011).
[90]S. Cerveny, J. Colmenero, and A. Alegrìa, J. Non-Cryst. Solids **353**, 4523 (2007).
[91]S. Cerveny, J. Mattsson, J. Swenson, and R. Bergman, J. Phys. Chem. B **108**, 11596 (2004).
[92]S. Cerveny, G. A. Schwartz, R. Bergman, and J. Swenson, Phys. Rev. Lett. **93**, 245702 (2004).
[93]F. Bruni, R. Mancinelli, and M. A. Ricci, Phys. Chem. Chem. Phys. **13**, 19773 (2011).
[94]J. H. Jan Swenson, Helén Jansson, and R. Bergman, J. Phys.: Condens. Matter **19**, 205109 (2007).
[95]F. Volino and A. Dianoux, Mol. Phys. **41**, 271 (1980).
[96]S. Jang, V. Molinero, T. Cagin, and W. Goddard, J. Phys. Chem. B **108**, 3149 (2004).
[97]J.-C. Perrin, S. Lyonnard, and F. Volino, J. Phys. Chem. C **111**, 3393 (2007).
[98]A. J. Moreno and J. Colmenero, Phys. Rev. E **74**, 021409 (2006).
[99]A. J. Moreno and J. Colmenero, J. Chem. Phys. **125**, 164507 (2006).
[100]J. Horbach, W. Kob, and K. Binder, Phys. Rev. Lett. **88**, 125502 (2002).
[101]J. Horbach and W. Kob, J. Phys.: Condens. Matter **14**, 9237 (2002).

This article is copyrighted as indicated in the article. Reuse of AIP content is subject to the terms at: http://scitation.aip.org/termsconditions. Downloaded to IP: 161.111.180.191 On: Fri, 05 Sep 2014 09:36:11

[102]C. Lorthioir, A. Alegría, and J. Colmenero, Phys. Rev. E **68**, 031805 (2003).
[103]J. Colmenero and A. Arbe, Soft Matter **3**, 1474 (2007).
[104]M. Laurati, P. Sotta, D. Long, L.-A. Fillot, A. Arbe, A. A. Alegría, J. P. Embs, T. Unruh, G. Schneider, and J. Colmenero, Macromolecules **45**, 1676 (2012).

[105]This behavior is opposite to the increase in intensity usually experienced by the first peak in fully deuterated samples. We note that the structural studies by NS are usually made on fully deuterated samples–when available–since (i) they reveal the 'true' structure factor (all atomic pair correlations equally weigthed) and (ii) the incoherent scattering is strongly reduced.

This article is copyrighted as indicated in the article. Reuse of AIP content is subject to the terms at: http://scitation.aip.org/termsconditions. Downloaded to IP: 161.111.180.191 On: Fri, 05 Sep 2014 09:36:11